Hindawi
Mathematical Problems in Engineering
Volume 2019, Article ID 9328326, 13 pages
https://doi.org/10.1155/2019/9328326

Research Article

Inversion Modeling of Dam-Zoning Elasticity Modulus for Heightened Concrete Dam Using ICS-IPSO Algorithm

Yijun Chen,[1,2,3] **Chongshi Gu**,[1,2,3] **Bangbin Wu**,[1,2,3] **Chenfei Shao**,[1,2,3] **Zhongru Wu**,[1,2,3] **and Bo Dai**[1,2,3]

[1]*College of Water Conservancy and Hydropower Engineering, Hohai University, Nanjing 210098, China*
[2]*State Key Laboratory of Hydrology-Water Resources and Hydraulic Engineering, Hohai University, Nanjing 210098, China*
[3]*National Engineering Research Center of Water Resources Efficient Utilization and Engineering Safety, Hohai University, Nanjing 210098, China*

Correspondence should be addressed to Yijun Chen; chen_yijun@hhu.edu.cn and Zhongru Wu; zrwu@hhu.edu.cn

Received 13 January 2019; Revised 27 February 2019; Accepted 21 March 2019; Published 9 April 2019

Academic Editor: Francesco Riganti-Fulginei

A new approach was developed for the inversion modeling of dam-zoning elasticity modulus for heightened concrete dam, with old and new concrete zones. The proposed inversion modeling procedure takes advantage of the improved cuckoo search (ICS) algorithm and improved particle swarm optimization (IPSO) algorithm to adjust the mechanical parameters, which are used as input. An objective function is constructed based on the horizontal displacement increment by using the finite element method (FEM) and statistical analysis of the prototype monitoring data. One ideal arch dam model and one actual heightened concrete dam were taken as examples. The proposed method was used to implement the optimal selection of the dam-zoning elasticity modulus. The inversion analysis results indicate that the mechanical parameters identification method for heightened concrete gravity dams proposed in this article is accurate and has a fast convergence rate. Consequently, it can be applied as a reliable model to identify the dam-zoning elasticity modulus in practical engineering applications.

1. Introduction

Due to the uneven geographical distribution of water resources and the need to alleviate the metropolitan water shortage in China, the water supply capacity of reservoirs is often increased by heightening dams or transferring water across regions. The new concrete dams are poured on the foundations of old dams that have been in service for many years, and thus there will exist new and old concrete zones in the dam body. A greater water pressure acts on the dam body as a result of the increasing reservoir water level. Furthermore, the structure response of a concrete dam is affected by many factors during its operation, including the dynamic and static cyclic water loading, ambient temperature, erosion, corrosion, crack, and so on. These influences are irreversible over the life cycle under complex environmental conditions [1, 2], which is mainly defined as the aging component in statistical regression analysis [3]. Therefore, the material property evolution of new and old concrete dam has an important impact on the working behavior of the heightened dam [4].

The material properties are generally reflected by the mechanical parameters, among which the reasonable determination of the elasticity modulus is very important to understanding the working state and evaluating the safety of a concrete dam [5]. The elasticity modulus can well represent the stiffness and resistance of the material, which can be applied to characterize the performance evolution of concrete structures [6]. Particularly in damaged dam structure, the identified elastic modulus can effectively reflect the presence of a structure deterioration process, but the damaged zone cannot be localized [1]. Thus, the elasticity modulus is the basis and prerequisite for the health diagnosis of a concrete dam. It is of great importance to adopt reasonable and effective methods to identify the elasticity modulus in old and new concrete zones during the normal operation period.

The elasticity modulus can be measured directly using core and rebound tests. Classical rebound tests are reliable but offer only a "pointwise" measurement in practice over concrete surfaces areas of a few square millimeters. Moreover, the mechanical parameters are very discrete for concrete dams that have been in service for many years, due to the cement paste, water cement ratio, cracks, corrosion, and carbonization in the concrete inside the dam body. The exact elasticity modulus of the concrete dam zones thus cannot be fully represented by the test method [7, 8].

Therefore, it is necessary to conduct an inversion analysis method to identify the mechanical parameters of the dam body, dam foundation, and reservoir basin on the basis of the dam prototype monitoring data analysis and structure simulation [9, 10]. However, the conventional inversion method can only identify the integrated elasticity modulus of the dam body, dam foundation, and reservoir basin. The dam body can be divided into different zones according to the material composition [11]. In recent years, various intelligent optimization algorithms have been applied to identify the mechanical parameters of concrete dams. Xiang introduced the genetic algorithm to obtain the elasticity modulus of the concrete dam and foundation [12]. Gu utilized the chaos genetic optimization algorithm [11] and the adjoint method combined with the DFP quasi-Newton method [13] to conduct the inversion analysis of the dam-zoning modulus in concrete dam, respectively. Fei proposed a parameter identification method for concrete dam-foundation systems based on statistical analysis of recorded dam displacements with a hybrid simplex artificial bee colony algorithm [14]. Dou adopted a novel adaptive fireworks algorithm to identify Young modulus of a concrete gravity dam and a concrete arch dam [15]. Nevertheless, from the inversion literature, it is inconsistent with the actual situation by using the absolute displacement of the prototype monitoring to conduct inversion analysis. Therefore, the inversion modeling of dam-zoning elasticity modulus has been proposed based upon the horizontal displacement increment.

Moreover, there have been very few studies addressing inversion problems on the zoning elasticity modulus of a heightened concrete dam. Even employing the cuckoo search (CS) optimization algorithm to obtain the mechanical parameters for the inversion analysis is currently one of the major gaps in the literature. In particularly, the deformation response of the heightened concrete dam is characterized by multiple extrema and nonlinearity, due to the many influencing factors and complicated influencing relations in the dam-water-foundation interaction. The CS algorithm has the advantages of simple and convenient operation, strong and stable global convergence ability, and good numerical stability in the process of extreme value optimization [16]. In this research, a new inversion modeling method was proposed to identify the dam-zoning elasticity modulus using the ICS-IPSO hybrid algorithm in a heightened concrete dam.

The paper is organized as follows: In Section 1, the background knowledge of the inversion analysis method is provided, including the CS optimization algorithm. Section 2 elaborates upon the separation method of the water pressure components using the hydraulic-thermal-time model, and an objective function is established. Section 3 describes the improved cuckoo search (ICS) algorithm and improved particle swarm optimization (IPSO) algorithm. The proposed inversion modeling is verified and illustrated by one ideal arch dam model and one actual heightened concrete dam project in Section 4. Finally, in Section 5, we draw some main conclusions.

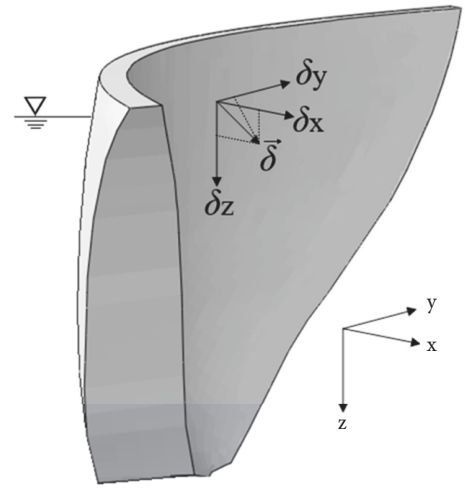

Figure 1: The displacement field of a concrete dam body.

2. Inversion Analysis Method of the Dam-Zoning Elasticity Modulus

2.1. Overview of the Hydraulic-Thermal-Time Statistical Model. The displacement field of the dam body generated at an arbitrary point is a vector field $\vec{\delta}$ under the action of the water pressure (H), ambient temperature (T), uplift pressure, sediment pressure, and other factors that can be decomposed into the radial horizontal displacement δ_x, side horizontal displacement δ_y, and vertical displacement δ_z, as shown in Figure 1. According to the mechanical theory analysis of the dam structure, the prototype measured displacement includes a reversible displacement and irreversible displacement. (1) The water pressure component δ_H and temperature component δ_T are the main components of the displacement, which are included in the reversible displacement. The water pressure component is mainly composed of the displacement caused by the reservoir water. The temperature component is caused by the temperature variation of the concrete hydration heat or the outside air temperature. (2) The irreversible displacement is mainly the aging component δ_θ. Furthermore, the water pressure component δ_H of the radial horizontal displacement δ_x can be used to identify the dam-zoning elasticity modulus. Therefore, the hydraulic-thermal-time statistical model of each component for the concrete dam radial horizontal displacement monitoring data is depicted in [17]

$$\begin{aligned}\delta_x &= \delta_H + \delta_T + \delta_\theta \\ &= a_0 + \sum_{i=1}^{n} a_i H^i + \sum_{i=1}^{m}\left(b_{1i}\sin\frac{2\pi it}{365} + b_{2i}\cos\frac{2\pi it}{365}\right) \\ &\quad + c_1\theta + c_2\ln\theta\end{aligned} \tag{1}$$

where a_0 is a constant term considering the influence of the initial state, a_i denotes the fitting coefficient of the water pressure, and H denotes the upstream water depth. According to the dam type, the value of n is different; for a concrete gravity dam, it is generally set to 3, while for an arch dam, it is 4 or 5. m denotes the period; $m = 1$ for an annual cycle, and $m = 2$ for a half-year cycle. b_{1i} and b_{2i} are fitting coefficients for the temperature. t is the cumulative day from the initial day to the present day. c_1 and c_2 are the fitting coefficients for the aging factor. θ takes a value of $t/100$.

2.2. The Objective Function Description. In an actual project, according to the structural function and material performance of a concrete dam, the dam body can be divided into different zones. According to the mathematical statistical model in (1), the water pressure component $\delta_{pw}^{\text{measure}}$ ($p = 1, 2, \ldots, P$, where P is the number of measuring points. $w = 1, 2, \ldots, W$, where W is the number of selected characteristic water levels) of the measured displacement in the dam prototype observation can be separated by adopting statistical regression analysis. The water pressure component increment $\Delta\delta_{pw}^{\text{measure}}$ at the p^{th} measuring point and w^{th} water level stage of the measured displacement can be obtained in (2). $\delta_{p0}^{\text{measure}}$ is the water pressure component at the initial water level. The calculated displacement $\delta_{pw}^{\text{inverse}}$ can be obtained by the finite element method under different characteristic water levels H_w ($w = 1, 2, \ldots, W$, where W is the number of characteristic water levels) in (3). The calculated displacement increment $\Delta\delta_{pw}^{\text{inverse}}$ at the p^{th} measuring point and w^{th} water level stage can be obtained by (4), where $\delta_{p0}^{\text{inverse}}$ is the calculated displacement at the initial water level. $E_i^{\text{inverse}} = (e_{i1}^{\text{inverse}}, e_{i2}^{\text{inverse}}, \cdots, e_{iz}^{\text{inverse}}) \in R^z$ ($i = 1, 2, \cdots, n$, where n is the number of nests in the CS algorithm or particles in the PSO algorithm and the parameter z is the number of zoning elasticity moduli on the basis of practical problems) is the design variable vector in z-dimensional space applied in the FEM analysis as calculation parameters, which represent the dam-zoning elasticity modulus updated by using the ICS-IPSO optimization algorithm.

$$\Delta\delta_{pw}^{\text{measure}} = \delta_{pw}^{\text{measure}} - \delta_{p0}^{\text{measure}} \tag{2}$$

$$\delta_{pw}^{\text{inverse}} = f\left(H_w, E_i^{\text{inverse}}\right) \tag{3}$$

$$\Delta\delta_{pw}^{\text{inverse}} = \delta_{pw}^{\text{inverse}} - \delta_{p0}^{\text{inverse}} \tag{4}$$

The horizontal displacement increments by using the finite element method (FEM) and statistical analysis of the prototype monitoring data are applied in inversion modeling to construct an objective function. A schematic diagram is shown in Figure 2. The water pressure component varying with the water level can be represented by line L_2, and the measured displacement can be collected by direct and reversed plumbs. However, the concrete dam is already under water loading H_{iniial} when the plumbs were installed in the dam body. Thus, the horizontal displacements monitored by the plumb system can only represent the relative displacement of the dam, rather than the absolute displacement. Hence, the horizontal displacement increment can be used in inversion analysis to identify the dam-zoning elasticity modulus.

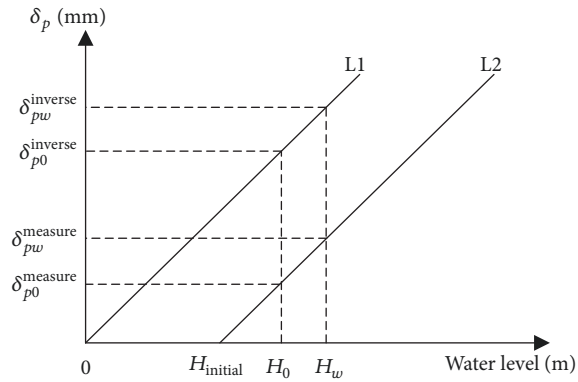

Figure 2: Schematic diagram of point p deformation in dam body with reservoir water level (L1: calculated displacement by FEM; L2: water pressure component of measured displacement).

The objective of the inversion model is to identify the optimal representation elasticity modulus of the dams. Consequently, the inversion problem can be transformed into the extremum optimization problem [18]. The objective function is constructed as follows:

$$\begin{aligned}&\text{minimize} \quad J = \frac{\sum_{p=1}^{P}\sum_{w=1}^{W}\left(\Delta\delta_{pw}^{\text{measure}} - \Delta\delta_{pw}^{\text{inverse}}\right)^2}{P \times W} \\ &\text{such that} \quad E_{\min} \le E_i^{\text{inverse}} \le E_{\max}\end{aligned} \tag{5}$$

where J denotes an objective function. $E_{\min}$ and $E_{\max}$ denote the lower and upper side constraints to the design variables, respectively, and the other symbols mean the same as above.

The concrete dam system composed of the dam body, rock foundation, and reservoir basin is divided into elements applying the finite element method. An equilibrium equation [19, 20] is established between the nodal displacement and nodal load as

$$[\boldsymbol{K}]\{\boldsymbol{\delta}\} = \{\boldsymbol{R}_H\} \tag{6}$$

where $[\mathbf{K}]$ denotes the overall stiffness matrix, $\{\boldsymbol{\delta}\}$ denotes the nodal displacement array, and $\{\mathbf{R}_H\}$ denotes the nodal force array. The expression $[K]$ can be represented as

$$\begin{aligned}[K] = &\sum_{e_j\in\Omega_1}[C]_{e_j}^T[K]_{e_j}[C]_{e_j} + \sum_{e_j\in\Omega_2}[C]_{e_j}^T[K]_{e_j}[C]_{e_j} \\ &+ \sum_{e_j\in\Omega_3}[C]_{e_j}^T[K]_{e_j}[C]_{e_j}\end{aligned} \tag{7}$$

where $\Omega_1, \Omega_2, \Omega_3$ are the computational domains of the dam body, rock foundation, and reservoir basin respectively. $[C]_{e_j}$ denotes the stiffness transformation matrix of element e_j. $[K]_{e_j}$ denotes the stiffness matrix of elemente_j, which can be represented as

$$[K]_{e_j} = \iiint_{\Omega_j} [B]^T [D] [B] \, d\Omega \tag{8}$$

where $[D]$ denotes the elastic matrix, which is related to the elasticity modulus E and Poisson ratio μ, and $[B]$ denotes the unit of the geometric characteristics, which are related to the element shape and size.

In this work, in particular, the difference in the objective function value between two adjacent iteration steps is defined to judge the convergence. Otherwise, the solution of the inversion analysis is complete when the number of iteration steps meets the requirements. The algorithm is iteratively checked until the specified convergence criterion of (9) is satisfied.

$$\frac{\left|J^T - J^{T-1}\right|}{J^T} \leq \varepsilon \quad \text{or } T > T^{\max} \tag{9}$$

where T denotes the iterative step, J^T denotes the objective function value during the T^{th} iteration, ε denotes the specified convergence tolerance, and $T^{\max}$ denotes the maximum number of iterations of the ICS-IPSO algorithm.

3. ICS-IPSO Hybrid Optimization Algorithm

3.1. Cuckoo Search (CS) Standard Algorithm. In this section, the cuckoo search algorithm is briefly reviewed. The CS is one of the latest nature-inspired metaheuristic algorithms, developed in 2009 by Xin-She Yang and Suash Deb [16]. The CS is based on the brood parasitism of some cuckoo species. Cuckoos lay their eggs in the nests of other host birds and remove the eggs of the host birds. The host birds may discover that the eggs are not its own, and either remove the foreign eggs or abandon the nest and build a new nest somewhere [21]. This algorithm is enhanced by using the so-called Lévy flights [22], rather than simple isotropic random walks. The long jumps may increase the search efficiency of the cuckoo search significantly in some cases, especially for multimodal, nonlinear problems. Each nest x_i is treated as a solution in a z-dimensional space, and the performance of each nest is evaluated according to a predefined fitness function, which is related to the solved problem.

For simplicity in describing the standard cuckoo search, the following three idealized rules were set:

(i) Each cuckoo lays one egg at a time and dumps it in a randomly chosen nest.

(ii) The best nests with high-quality eggs will be carried over to the next generations.

(iii) The number of available host nests is fixed, and the egg laid by a cuckoo is discovered by the host bird with a probability $p_a \in (0, 1)$. In this case, the host bird either gets rid of the eggs or simply abandons the nest and build a completely new nest.

Furthermore, the CS algorithm uses a balanced combination of a local random walk and the global explorative random walk, controlled by a switching parameter p_a [16, 21]. The local random walk can be written as

$$x_i^{T+1} = x_i^T + \alpha s \otimes H\left(p_a - \varepsilon\right) \otimes \left(x_j^T - x_k^T\right) \tag{10}$$

where the superscript T denotes the T^{th} iteration. $\alpha, \varepsilon \in (0, 1)$ are random numbers drawn from a uniform distribution, s is the step size, and $H(p_a - \varepsilon)$ is a Heaviside function. x_j^T and x_k^T are two different solutions selected randomly by random permutation in the T^{th} iteration, and the product $\otimes$ represents entry-wise multiplication.

On the other hand, the global random walk is carried out by adopting Lévy flights.

$$x_i^{T+1} = x_i^T + \alpha L\left(s, \lambda\right) \tag{11}$$

where

$$L\left(s, \lambda\right) = \frac{\lambda \Gamma\left(\lambda\right) \sin\left(\pi\lambda/2\right)}{\pi} \frac{1}{s^{1+\lambda}}, \left(s \longrightarrow +\infty\right) \tag{12}$$

Here, $\alpha > 0$ denotes the step size scaling factor, which should be related to the scale of the problem of interest. In most cases, we can use $\alpha = O(L/10)$, where L is the characteristic scale of the problem of interest, while in some cases, $\alpha = O(L/10)$ can be more effective to avoid flying too far. Obviously, the α value in these two updating equations can be different, thus leading to two different parameters α_1 and α_2. Here, we use $\alpha_1 = \alpha_2 = \alpha$ for simplicity. $L(s, \lambda)$ denotes the step-lengths that are distributed according to the probability distribution shown in (12), which has an infinite variance with an infinite mean.

However, generating a pseudorandom step size s using Lévy flights is not trivial. The most effective and direct method is to adopt the Mantegna algorithm to achieve symmetric Lévy flights, and the step size can be calculated in (13). The two variables U and V are drawn from Gaussian distributions that are depicted in (14) and (15) [21, 22].

$$s = \frac{U}{|V|^{1/\lambda}}, \quad (1 < \lambda \leq 3) \tag{13}$$

where

$$\begin{aligned} U &\sim N\left(0, \sigma^2\right), \\ V &\sim N\left(0, 1\right) \end{aligned} \tag{14}$$

$$\sigma^2 = \left[\frac{\Gamma\left(1 + \lambda\right)}{\lambda \Gamma\left(\left(1 + \lambda\right)/2\right)} \cdot \frac{\sin\left(\pi\lambda/2\right)}{2^{(\lambda-1)/2}}\right]^{1/\lambda} \tag{15}$$

3.2. Improved Cuckoo Search (ICS) Algorithm. The parameter p_a introduced in the CS algorithm helps the local random walk to update solutions, which can influence the convergence rate and the precision of the solutions [23]. In general, the CS standard algorithm uses a fixed value for p_a, and the

value is set in the initialization step and cannot be changed during new generations, which may result in premature convergence.

To keep the balance between global and local searches and increase the population evolution intensity, a variable parameter P_a is introduced to adjust the value of the switching parameter. In addition, the value of P_a should be decreased with the search progress to more easily produce new individuals at the later iteration stage to avoid falling into local optima, which can be presented as follows:

$$P_a(T) = P_{a,\max} - \frac{\left(P_{a,\max} - P_{a.\min}\right)}{T^{\max}} \times T \tag{16}$$

where $T^{\max}$ denotes the maximum iterative steps, T denotes the current iteration step, and $P_{a,\max}$ and $P_{a,\min}$ denote the control probability of the switching parameter P_a.

3.3. Improved Particle Swarm Optimization (IPSO) Algorithm. To further enhance the global and local exploration capability and improve the convergence rate, as well as avoid the premature convergence of the algorithm, the IPSO algorithm is integrated into the ICS algorithm. Particle swarm optimization (PSO) is a parallel evolutional computation technique developed by Kennedy and Eberhart based on the simulation of the social behavior of birds in a flock [24, 25]. The new velocity v_i of particle i is determined by adjusting its previous velocity based on the distance of its current position from its best position in (17). Then, the position x_i of particle i is updated according to its companion and own flying experience, which is treated as a point in z-dimensional space according to the material zoning of the practical project in (18). p_i denotes the best previous position that particle i has ever visited, and the value of p_g denotes the best particle among all the particles in the population. The performance of each particle is evaluated according to a predefined fitness function, which is related to the solved problem.

$$v_i^{T+1} = wv_i^T + c_1 r_1 \left(p_i^T - x_i^T\right) + c_2 r_2 \left(p_g^T - x_i^T\right) \tag{17}$$

$$x_i^{T+1} = x_i^T + \alpha v_i^{T+1} \tag{18}$$

where the superscript T denotes the T^{th} iteration. w denotes the inertia weight, which is employed to control the impact of the previous velocities on the current velocity. c_1 and c_2 are positive constants, called the cognitive and social parameters, respectively. r_1 and r_2 are random numbers uniformly distributed in the range (0,1). α represents a scaling factor that controls the velocity of the particles.

The appropriate inertia weight w can influence the trade-off between the global and local exploration abilities of the "flying points". A larger inertia weight can facilitate the global exploration ability, while a smaller inertia weight can effectively improve the ability of local exploration, thereby improving the search precision of the algorithm and finding the optimal solution more quickly and accurately. Particularly, in this research, the inertia weight w is dynamically changed along with the algorithm optimization process to provide a balance between the global and local exploration abilities and increase the convergence rate [25]. The inertia weight is expressed in (19). The advantages of the function are as follows. (1) The function is monotonically decreasing in the region, which meets the requirement of a large inertia weight at the beginning and a small inertia weight at the end. (2) The decreasing speed of this function is relatively slow at the beginning, which is conducive to exploring the optimal solution and avoid getting stuck in local optima. (3) The function maintains a relatively flat decreasing speed at the end, which is conducive to facilitating the local search and improving the search precision [26].

$$w(T) = \frac{w_{\max} - w_{\min}}{2} \times \cos\left(\frac{\pi \times T}{T^{\max}}\right) + \frac{w_{\max} + w_{\min}}{2} \tag{19}$$

where $w_{\max}$ and $w_{\min}$ are the maximum and minimum inertia weight w, respectively, $T^{\max}$ is the maximum number of iteration steps, and T denotes the current iteration step.

3.4. Steps for Implementing the Inversion Analysis Method. According to the above descriptions of the ICS algorithm and IPSO algorithm, the execution process of the dam-zoning elasticity modulus inversion analysis method using the ICS-IPSO optimization algorithm is mainly composed of three parts. First, the global random walk is carried out by adopting Lévy flights, instead of simple isotropic random walks. Then, the switching parameter P_a is dynamically changed with the CS algorithm optimization progress to update the local position of the nest. Third, a monotonically decreasing inertia weight w is applied in the PSO algorithm to facilitate global exploration in the early stage, while a smaller inertia weight enhances the local exploration ability in the later stage. The model structure and operating process are shown in Figure 3 and have been implemented on the MATLAB platform. The strategy for implementing the dam-zoning elasticity modulus inversion analysis method is described as follows.

Step 1. Set the parameters of the ICS-IPSO optimization algorithm. Namely, ε, $T^{\max}$, $E_{\min}$, $E_{\max}$, n, $P_{a,\max}$, $P_{a,\min}$, $w_{\max}$, $w_{\min}$, c_1, and c_2 are set to 1×10^{-32}, 40, 20, 40, 10, 0.25, 0.005, 0.8, 0.4, 1.5, and 1.5, respectively. The parameter z represents the dimensional space of each nest or particle, which is determined according to the number of material partitions in the actual project. Input the measured displacement increment dataset $\Delta\delta_{pw}^{\text{measure}}$ obtained from the dam body, which will be applied in the objective function to evaluate the performance of each nest or particle.

Step 2. Generate the random initial vector values of the nests $E_i^0 = (e_{i1}^0, e_{i2}^0, \cdots, e_{iz}^0) \in R^z$ $(i = 1, 2, \ldots, n)$ in the constraint condition equation (5) and the iteration step $T = 0$. The displacement of typical points in the FEM model will be recomputed using each nest E_i^0 as elasticity modulus in the calculation parameters in (3). Evaluate the fitness value J_i^0 of each nest in (5), and record the best individual E_g^0 with the best fitness value J_g^0.

Step 3. Update the iteration number $T = T+1$. Each nest $E_i^T = (e_{i1}^T, e_{i2}^T, \cdots, e_{iz}^T) \in R^z$ is updated by adopting Lévy flights in

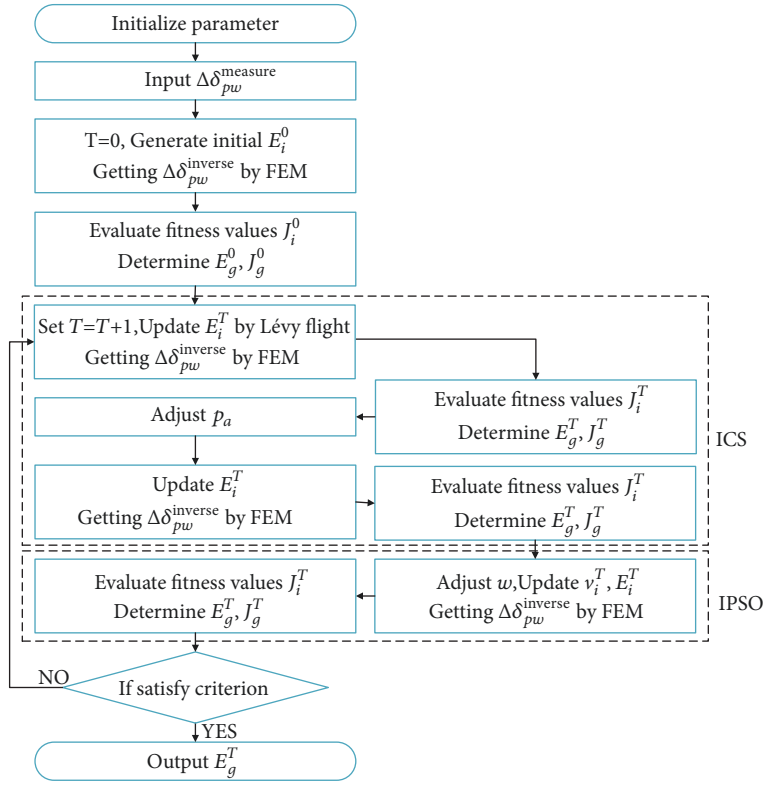

Figure 3: Flowchart of the inversion analysis method of dam-zoning elasticity modulus using the ICS-IPSO algorithm.

(8). The displacement of typical points in the FEM model will be recomputed using each nest E_i^T as elasticity modulus in the calculation parameters in (3). Evaluate the fitness value J_i^T of each nest in (5), and determine the best individual E_g^T with the best fitness value J_g^T.

Step 4. Equation (16) is used to calculate the dynamic switching parameter p_a. Equation (10) is applied to abandon the worst nests and build new nests $E_i^T = (e_{i1}^T, e_{i2}^T, \cdots, e_{iz}^T) \in R^z$. The displacement of typical points in the FEM model will be recomputed using each nest E_i^T as elasticity modulus in the calculation parameters in (3). Evaluate the fitness value J_i^T of each nest in (5), and record the best individual E_g^T with the best fitness value J_g^T.

Step 5. Equation (19) is utilized to calculate the dynamic inertia weight w and change the velocity and position $E_i^T = (e_{i1}^T, e_{i2}^T, \cdots, e_{iz}^T) \in R^z$ of the particles according to (17) and (18), respectively. The displacement of the typical points in the FEM model will be recomputed using each nest E_i^T as elasticity modulus in the calculation parameters in (3). Evaluate the fitness value J_i^T of each nest in (5), and record the best individual E_g^T with the best fitness value J_g^T.

Step 6. If the convergence criterion in (9) is satisfied, then output the optimal solution E_g^T. Otherwise, loop to Step 3 for the next iteration.

4. Numerical Examples

In this section, two examples are considered. In the first example, the target displacement of the ideal concrete arch dam prescribed elasticity modulus is carried out to verify the capability of the proposed dam-zoning elasticity modulus inversion analysis method using the ICS-IPSO algorithm. In the second example, to further verify the practicability of the inversion analysis method, a practical project is considered to inverse the elasticity modulus of the dam body and dam foundation under the actual working conditions.

4.1. Case 1: Concrete Arch Dam Subjected to Prescribed Elasticity Modulus. In the following example, the feasibility and effectiveness of the ICS-IPSO algorithm in the dam-zoning elasticity modulus inversion analysis are verified, and the strategy is detailed as follows.

In this case, the prescribed dam-zoning elasticity modulus $E^{specify} \in R^2$ for two materials zones and boundary conditions, as well as the water level, that are applied to produce a desired deformation of an ideal concrete arch dam, can be identified based on the proposed inversion modeling. The 3D finite element model is discretized by 22384 elements and 25836 nodes. The concrete arch dam is 305 m high and is subjected to 300 m of hydrostatic pressure. The finite element model and material partition are depicted in Figure 4. The prescribed elasticity modulus $E^{specify} = (30.55, 24.55)$ GPa, Poisson's ratio, and density for each material zones used in this analysis are listed in Table 1. A schematic diagram of

Table 1: Real parameters for concrete material and the inversion elasticity modulus.

Zone	γ(KN/m^3)	μ	E^{specify}(GPa)	E^{inverse}(GPa)	$\left\|E^{\text{specify}} - E^{\text{inverse}}\right\|_2$
Zone B	2450	0.167	30.55	30.546	0.0064
Zone C	2700	0.220	24.55	24.545	

Note: γ denotes water density. μ denotes Poisson's ratio.

Table 2: Displacement of a typical measuring point (mm).

Typical point	Point 1	Point 2	Point 3	Point 4	Point 5	Point 6
δ^{real}	60.8940	64.4630	62.9560	55.5300	36.1290	7.8617
δ^{inverse}	60.9030	64.4730	62.9650	55.5380	36.1350	7.8631

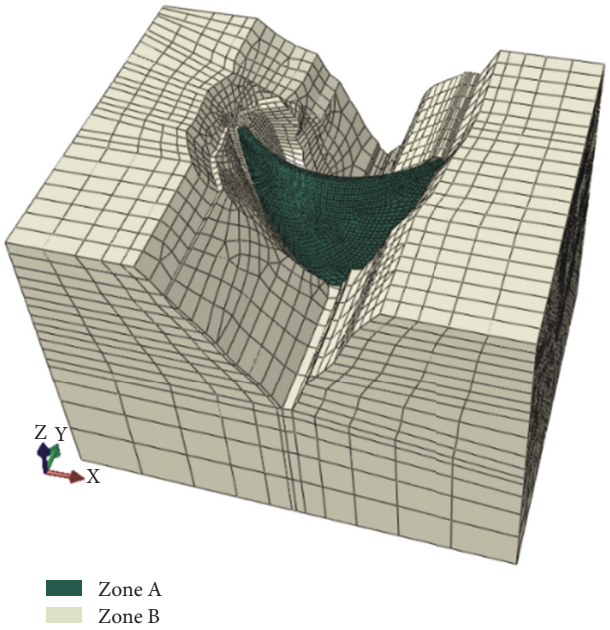

Figure 4: 3D finite element mesh for ideal concrete arch dam.

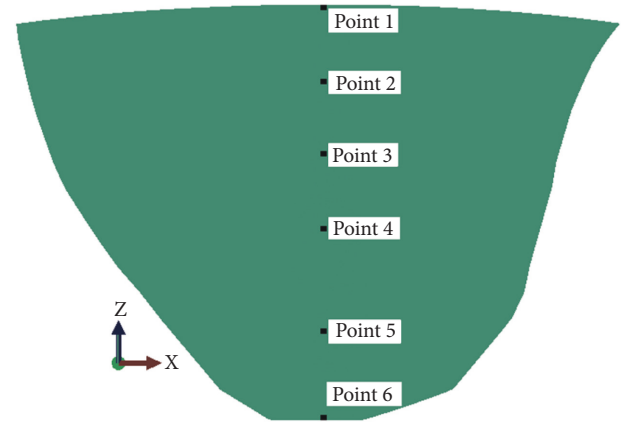

Figure 5: Schematic diagram of the positions of typical points in the arch dam body.

the positions of the typical points in the arch dam body is depicted in Figure 5, and the displacement values δ^{real} of selected typical points are shown in Table 2. The deformation of the dam body using the prescribed elasticity modulus is shown in Figure 6(d).

An inversion analysis on the basis of the target configuration is carried out. The reconstructed deformations of the representative iterations are shown in Figures 6(a), 6(b), and 6(c). Figure 7 displays the zoning elasticity modulus variation over the inversion process. The moving process of optimizing the elasticity modulus is shown in Figure 8. The convergence of the objective functions and elasticity modulus L2 error norm determined by (20) over the iterations is illustrated in Figures 9 and 10, respectively. The inversion solutions $E^{\text{inverse}} = (30.546, 24.545)$ GPa are obtained when the iteration steps reach 40, as shown in Table 1. The displacement values δ^{inverse} of selected typical points are shown in Table 2.

As the results indicate, it is clear that the inversion elasticity modulus E^{inverse} is in good agreement with E^{specify}. E_{error} is 0.0064, which implies that the proposed model is reasonable and precise. The objective function value between the real displacement δ^{real} and the inversion displacement δ^{inverse} is 5.06×10^{-29} during iteration 40. Therefore, the results indicate that the dam-zoning elasticity modulus inversion analysis method using the ICS-IPSO algorithm is feasible and effective.

$$E_{error} = \sum_{r=1}^{z} \sqrt{E_r^{\text{inverse}} - E_r^{\text{specify}}} \tag{20}$$

where z is the number of material partitions. In this case, $z = 2$.

4.2. Case 2: Inversion Analysis of Elasticity Modulus for Heightened Concrete Gravity Dams

4.2.1. General Situation. A hydropower station is located at the junction of the Han river and its tributary Danjiangkou river, in Danjiangkou city, Hubei Province, China. It is a heightened concrete gravity dam project constructed in two

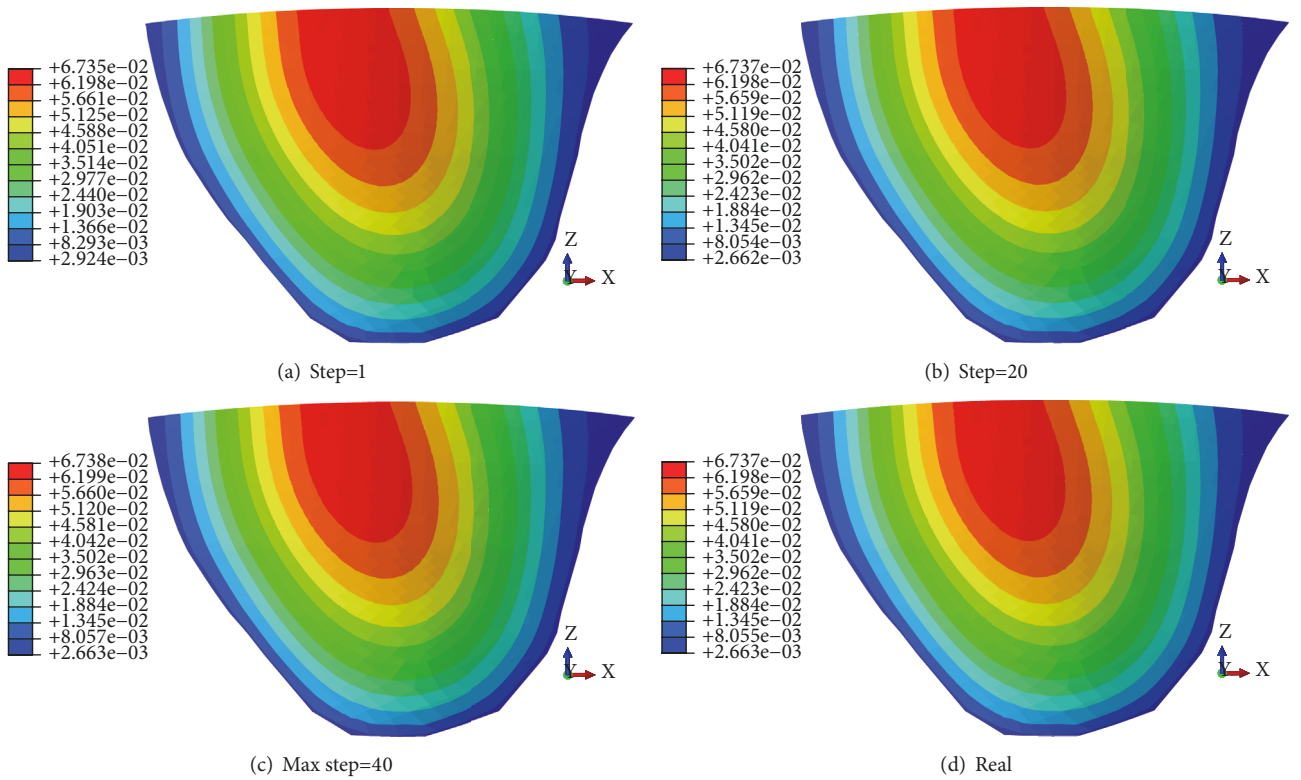

Figure 6: The Y-displacement over the inversion process. (a) The reconstructed deformation at the first iteration. (b) The reconstructed deformation at the 20th iteration. (c) The reconstructed deformation at the 40th iteration. (d) The deformation using the prescribed elasticity modulus.

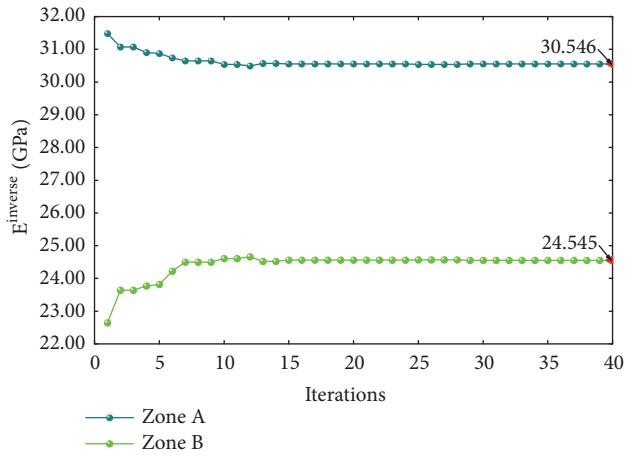

Figure 7: The zoning elasticity modulus variation during the inversion process.

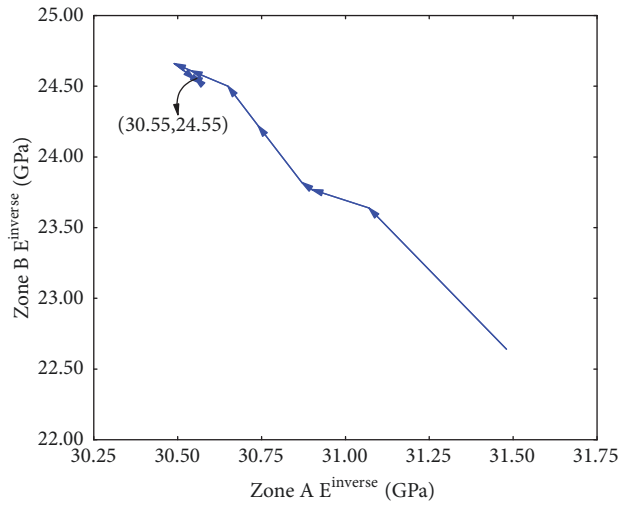

Figure 8: The moving process of optimizing the elasticity modulus.

phases. It is the key project to develop and control the Han river with comprehensive utilization benefits of flood control, water supply, power generation, and shipping. In addition, it is also the source of water for the middle route of the South-North Water Diversion Project.

For the first phase, the concrete dam construction began in September 1958 and finished in December 1973. The crest elevation is 162.00 m, the crest length is 1141 m, the foundation surface is 81.90 m, and the dam height is 80.10 m. The width of each dam section is 24 m along the axis of the dam. The normal water level is 157.00 m. The concrete gravity dam is divided into 58 sections. According to the function of the concrete gravity dam, the dam body is divided into the right bank joins section, deep hole spillway section, shallow hole overflow section, powerhouse section, and left bank joins

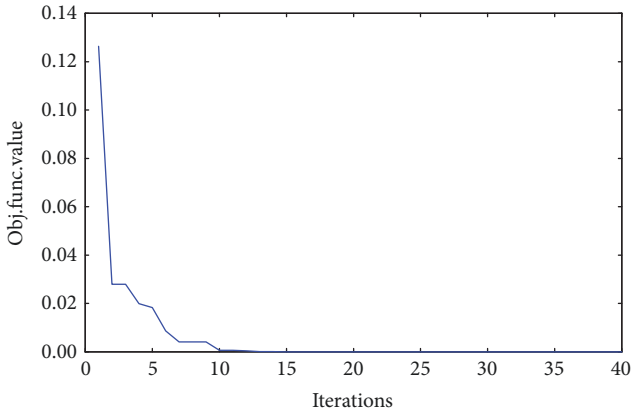

Figure 9: The objective function versus the number of iterations.

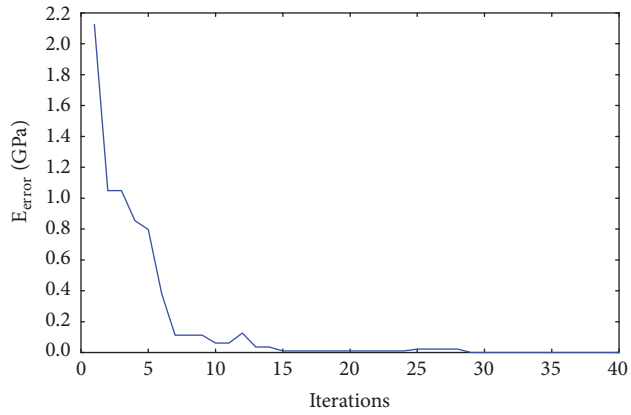

Figure 10: Convergence of L^2 error norm in parameter space elasticity modulus versus the number of iterations.

section. For the second phase, to implement cross-regional water diversion plans to solve the problem of water shortages, the concrete dam needed to be further poured to increase the storage capacity. In September 2005, the concrete dam project was constructed again, and the second phase finished in March 2010. The crest elevation is 176.60 m after the heightening, an increase of 14.60 m compared with the initial dam project. The normal reservoir level is 170.00 m above sea level. The total storage capacity of the reservoir is 33.91 billion m^3, with its main purpose being water supply.

This case focused on the inversion analysis method as applied to the heightened concrete dam project conducted in two phases. Therefore, the 13# dam section will be considered in this case, which is deep hole spillway section and located in the middle of the riverbed. The established model is composed of a total of 135232 elements and 146122 nodes, including 11376 elements and 12975 nodes for the new concrete dam (zone A), and 48328 elements and 53984 nodes for the old concrete dam (zone B); zone C is the dam foundation. The model and boundary conditions are illustrated in Figure 11. The direct plumbs are installed in the dam body to measure the dam horizontal displacement, the measuring points PL1-1 and Pl1-2 are arranged in zone A, and the measuring points PL2-1, PL2-2, and PL2-3 are arranged in zone B, as shown in Figure 12.

4.2.2. Inversion Analysis of Elasticity Modulus. The statistical model in (1) is used to separate the displacements of the water pressure component, temperature component, and aging component, based on the measured displacement of the corresponding measuring points. The water pressure component will be applied in this case to identify the dam-zoning elasticity modulus. Figure 13 shows the measured upstream water level and radial displacement separation results of measuring point PL2-3 in the old concrete dam (Zone B) from June 1, 2013, to December 31, 2017, during which a total of 72 groups of data were accumulated. Negative values denote the radial horizontal displacement upstream. The displacement separation results of the other measuring points are similar to those above and will not be described here.

According to the time series characteristics of the water level and the principle that the period of the sudden rise of the reservoir water level should be selected as the inversion analysis period, the period from August 24, 2017, to October 19, 2017, was selected as the inversion period in this case, as shown in Figure 13. The water pressure component under different characteristic water levels of 157.79, 161.76, 164.56, and 166.34 m is input as $\delta_{pw}^{\text{measure}}$ in (2). The ICS-IPSO algorithm is introduced to update the dam-zoning elasticity modulus, which is E_i^{inverse} in (3). The displacements $\delta_{pw}^{\text{inverse}}$ in (3) can be calculated under different characteristic water levels of 157.79, 161.76, 164.56, and 166.34 m by adopting the finite element method based on the updated elasticity modulus E_i^{inverse}. In this case, the range values of the elasticity modulus inversion analysis are [20, 40] GPa as the constraint condition in (5). The zoning elasticity modulus variation during the inversion process can be seen in Figure 14. The real parameters for the concrete material and the inversion result of the dam-zoning elasticity modulus $E^{\text{inverse}} = (36.46, 30.53, 24.17)$ GPa are shown in Table 3. The measured displacements increment $\Delta\delta_{pw}^{\text{measure}}$ and calculated displacements increment $\Delta\delta_{pw}^{\text{inverse}}$ by the inversion analysis of the measuring points under different characteristic water levels are displayed in Table 4. To verify the efficiency of the ICS-IPSO algorithm, the CS standard algorithm, PSO standard algorithm, and ICS, ICS-PSO were also used for the inversion analysis. The optimization objective function over the iterations is displayed in Figure 15, and the objective function value of the ICS-IPSO hybrid algorithm is 2.35×10^{-31} during iteration 40. Hence, the convergence rate of the ICS-IPSO hybrid algorithm is quicker than that of the other algorithms.

To verify the correctness of the inversion analysis results, the period from October 15, 2017, to December 27, 2017, was selected as the verification stage, as shown in Figure 13. Utilizing the elasticity modulus E^{inverse} in Table 3 as the calculation parameters, the radial horizontal displacements were calculated by the finite element method under different characteristic water levels of 166.74, 166.01, and 165.52 m, as shown in Table 5. A comparison of the measured displacement increment $\Delta\delta_{pw}^{\text{measure}}$ and calculated displacement

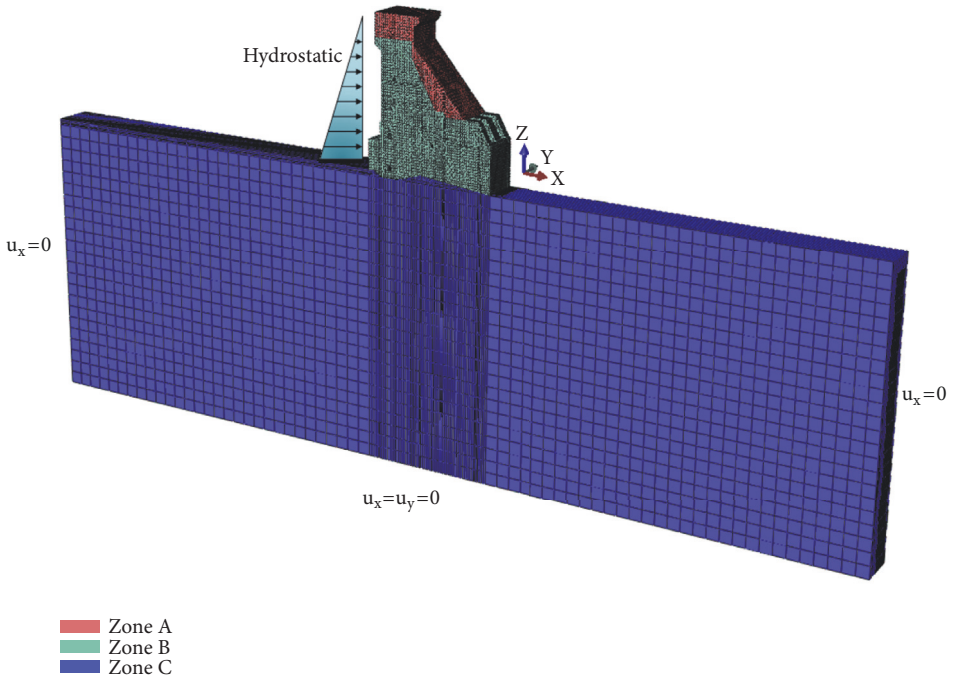

Figure 11: 3D finite element mesh for 13# dam section of Danjiangkou project.

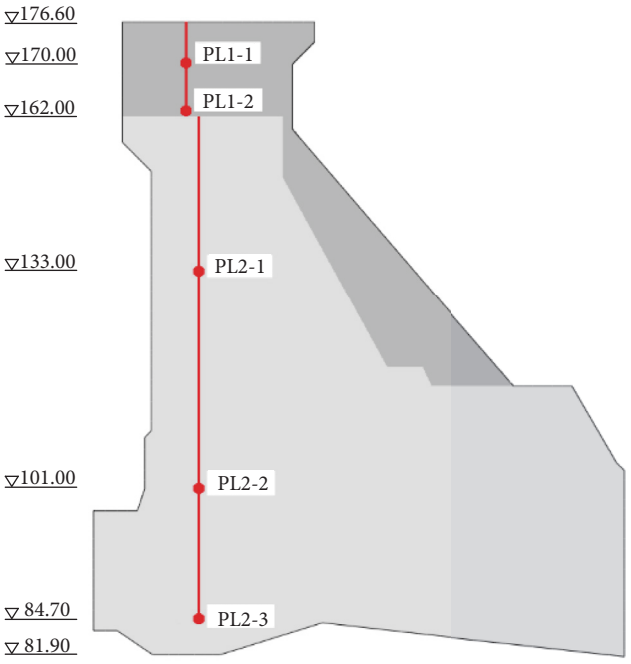

Figure 12: Arrangement diagram of the measuring points and the direct plumbs in the 13# dam section.

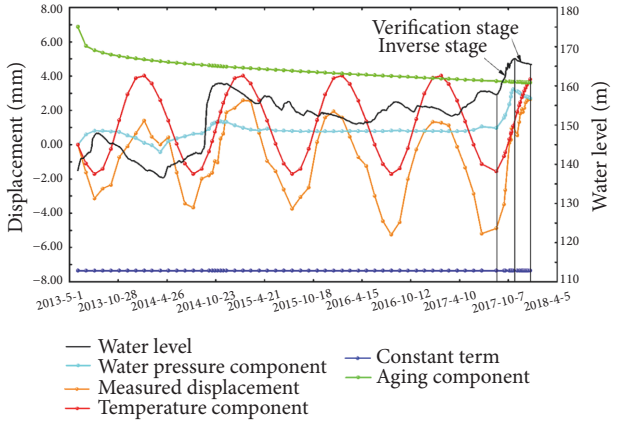

Figure 13: Time curves of monitored and separated displacements of the PL2-3 measuring point.

increment $\Delta\delta_{pw}^{\text{inverse}}$ can be seen in Table 5. The comparison of the calculated displacements and measured displacements of the measuring points under different characteristic water levels of 166.74, 166.01, and 165.52 m is shown in Figure 16. As seen from Table 5 and Figure 16, the calculated displacements have good correspondence with the measured displacements under the series of water loads. Consequently, the inversion results of the zoning elasticity modulus are rational in this case, and the practicability of the proposed inversion analysis method is verified.

5. Conclusions

This paper presents the inversion analysis strategy to obtain the dam-zoning elasticity modulus in a heightened concrete

Table 3: Real parameters for concrete material and the zoning elasticity modulus inversion.

Zone	γ(KN/m^3)	μ	$E^{inverse}$(GPa)
Zone A (new concrete dam)	2450	0.167	36.46
Zone B (old concrete dam)	2450	0.167	30.53
Zone C (rock)	2700	0.220	24.17

Table 4: A comparison of the measured displacements and identified displacements obtained by the inversion analysis of typical measuring points at different water levels (mm).

Displacements	$\Delta\delta_{pw}^{measure}$			$\Delta\delta_{pw}^{inverse}$		
Date	2017/9/21	2017/10/11	2017/10/19			
Water level	161.76	164.56	166.34	161.76	164.56	166.34
PL1-1	0.069	0.127	0.170	0.070	0.127	0.167
PL1-2	0.153	0.284	0.376	0.157	0.286	0.377
PL2-1	0.269	0.487	0.633	0.265	0.483	0.636
PL2-2	0.625	1.116	1.457	0.621	1.117	1.458
PL2-3	0.759	1.355	1.766	0.759	1.359	1.770

Note: in this case, the reservoir water level of 157.79 m on August 24, 2017, was used as the initial water level H_0.

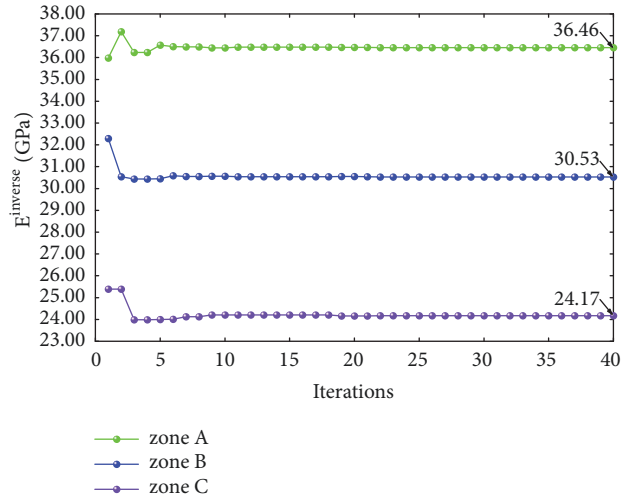

Figure 14: The zoning elasticity modulus variation during the inversion process.

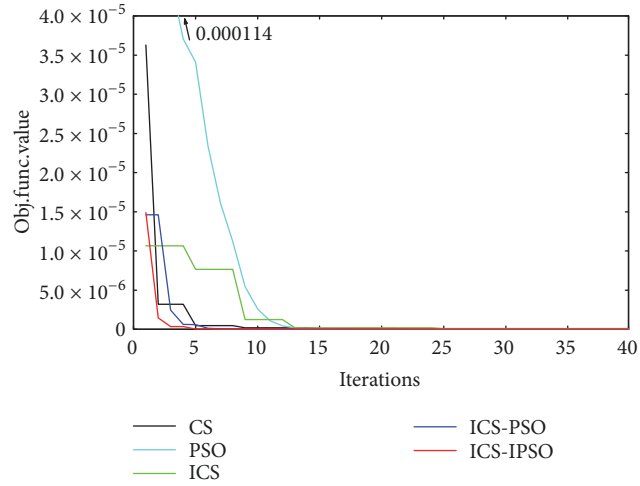

Figure 15: The objective function versus the number of iterations.

dam combining statistical analysis of the prototype monitoring data and the ICS-IPSO hybrid optimization algorithm. Furthermore, an objective function is constructed based on the horizontal displacement increment. The conclusions obtained are as follows:

(1) The proposed method is used to identify the dam-zoning elasticity modulus for the ideal arch dam model prescribed elasticity modulus in case 1. It has to be stated that the investigated example shows high performance for the inversion modeling. Consequently, it can be concluded that the ICS-IPSO hybrid algorithm has been successfully verified as an effective method for inverse analysis of dam-zoning elasticity modulus.

(2) Taking a concrete gravity dam that is heightened in stages as an example in case 2, the inversion modeling on the basis of the ICS-IPSO is successfully adopted to identify the elasticity modulus in new and old concrete zones. In addition, the identified mechanical parameters can be utilized to accurately calculate the future displacement of the dam using the FEM.

(3) The CS, PSO, ICS, and ICS-PSO algorithms are also employed to conduct an inversion analysis in case 2. The results show that the ICS-IPSO has the advantages of a fast convergence rate and more stable search results. The inversion modeling proposed in this paper can also be applied to other heightened concrete dam problems. It also has the power to deal with the problems with more zones of the concrete dam because of the global search ability.

Table 5: A comparison of the measured displacements and calculated displacements of typical measuring points at different water levels (mm).

Displacements	$\Delta\delta_{pw}^{measure}$			$\Delta\delta_{pw}^{inverse}$		
Date	2017/10/25	2017/11/26	2017/12/27			
Water level	166.74	166.01	165.52	166.74	166.01	165.52
PL1-1	0.173	0.157	0.145	0.177	0.160	0.148
PL1-2	0.403	0.359	0.336	0.399	0.360	0.334
PL2-1	0.677	0.610	0.566	0.672	0.607	0.564
PL2-2	1.538	1.388	1.300	1.537	1.393	1.298
PL2-3	1.861	1.687	1.578	1.865	1.692	1.578

Note: in this case, the reservoir water level of 157.79 m on August 24, 2017, was used as the initial water level H_0.

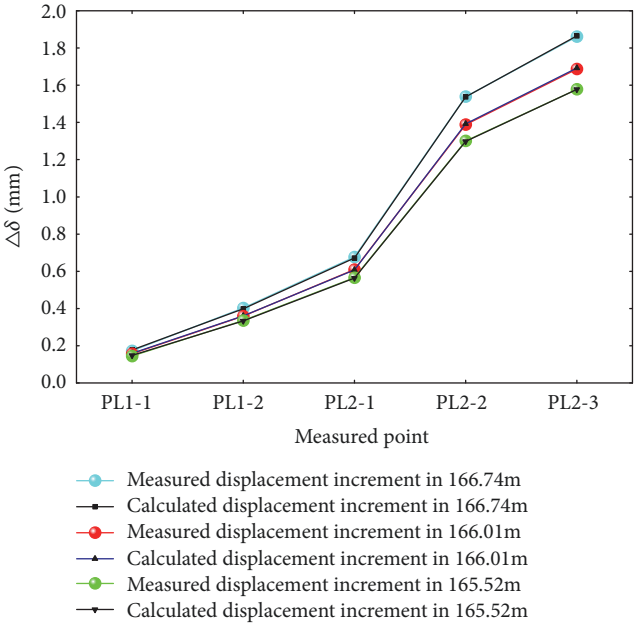

Figure 16: Comparison between the measured and calculated displacement increments of typical measuring points at different water levels.

Data Availability

The data used to support the findings of this study have not been made available.

Conflicts of Interest

The authors declare that they have no conflicts of interest regarding the publication of this paper.

Acknowledgments

The authors would like to acknowledge the research funds supported by National Key R&D Program of China (2016YFC0401601, 2018YFC0407104, 2018YFC1508603, and 2018YFC0407101), National Natural Science Foundation of China (Grants nos. 51739003, 51579085, 51779086, 51579086, 51379068, 51579083, and 51609074), Project Funded by the Priority Academic Program Development of Jiangsu Higher Education Institutions (YS11001), Special Project Funded of National Key Laboratory (20165042112), and Key R&D Program of Guangxi (AB17195074).

Supplementary Materials

Case 1: column A and column B of data are used to draw Figures 7 and 8, which display the zoning elasticity modulus variation over the inversion process and the moving process of optimizing elasticity modulus. Column D of data is used to draw Figure 10, which displays the objective function versus the number of iterations. Column F of data is used to draw Figure 9, which displays the convergence of L2 error norm in parameter space elasticity modulus versus the number of iterations. Case 2: columns A, B, and C of data in sheet inversion are used to draw Figure 14, which display the zoning elasticity modulus variation over the inversion process. Columns A, B, C, D, and E of data in sheet fun are used to draw Figure 15, which display the objective function versus the number of iterations. *(Supplementary Materials)*

References

[1] A. de Sortis and P. Paoliani, "Statistical analysis and structural identification in concrete dam monitoring," *Engineering Structures*, vol. 29, no. 1, pp. 110–120, 2007.

[2] B. Wu, Z. Wu, B. Chen, H. Su, T. Bao, and S. Wang, "Crack status analysis for concrete dams based on measured entropy," *Science China Technological Sciences*, vol. 59, no. 5, pp. 777–782, 2016.

[3] Z. Wu and C. Gu, *Hidden Trouble Detection and Health Diagnosis of Large Hydraulic Concrete Structure*, Higher Education Press, Beijing, China, 2005.

[4] R. Ardito, G. Maier, and G. Massalongo, "Diagnostic analysis of concrete dams based on seasonal hydrostatic loading," *Engineering Structures*, vol. 30, no. 11, pp. 3176–3185, 2008.

[5] M. Hassoun and A. Al-Manaseer, *Structural Concrete: Theory and Design*, John Wiley & Sons, New Jersey, NJ, USA, 2012.

[6] B. Ahmadi-Nedushan, "Prediction of elastic modulus of normal and high strength concrete using ANFIS and optimal nonlinear regression models," *Construction and Building Materials*, vol. 36, pp. 665–673, 2012.

[7] B. Sevim, A. C. Altunişik, A. Bayraktar, M. Akköse, and S. Adanur, "Estimation of elasticity modulus of a prototype arch

dam using experimental methods," *Journal of Materials in Civil Engineering*, vol. 24, no. 4, pp. 321–329, 2012.

[8] J. Vilardell, A. Aguado, L. Agullo, and R. Gettu, "Estimation of the modulus of elasticity for dam concrete," *Cement and Concrete Research*, vol. 28, no. 1, pp. 93–101, 1998.

[9] D. Zheng, L. Cheng, T. Bao, and B. Lv, "Integrated parameter inversion analysis method of a CFRD based on multi-output support vector machines and the clonal selection algorithm," *Computers & Geosciences*, vol. 47, pp. 68–77, 2013.

[10] R. Ardito, P. Bartalotta, L. Ceriani, and G. Maier, "Diagnostic inverse analysis of concrete dams with statical excitation," *Journal of the Mechanical Behavior of Materials*, vol. 15, no. 6, pp. 381–389, 2004.

[11] H. Gu, Z. Wu, X. Huang, and J. Song, "Zoning modulus inversion method for concrete dams based on chaos genetic optimization algorithm," *Mathematical Problems in Engineering*, vol. 2015, Article ID 817241, 9 pages, 2015.

[12] Y. Xiang, H. Su, and Z. Wu, "Inverse analysis of mechanical parameters based on dam safety monitoring data," *Journal of Hydraulic Engineering*, vol. 35, no. 8, pp. 98–102, 2004 (Chinese).

[13] H. Gu, Z. Wu, X. Huang, J. Song, and L. Z. Sun, "Dam-zoning modulus reconstruction using adjoint method," *European Journal of Environmental and Civil Engineering*, vol. 22, no. 9, pp. 1089–1110, 2018.

[14] F. Kang, J. Li, and Q. Xu, "Structural inverse analysis by hybrid simplex artificial bee colony algorithms," *Computers & Structures*, vol. 87, no. 13-14, pp. 861–870, 2009.

[15] S. Dou, J. Li, and F. Kang, "Parameter identification of concrete dams using swarm intelligence algorithm," *Engineering Computations*, vol. 34, no. 7, pp. 2358–2378, 2017.

[16] X. Yang and S. Deb, "Cuckoo Search via Lévy flights," in *Proceedings of the World Congress on Nature & Biologically Inspired Computing (NaBIC '09)*, pp. 210–214, IEEE, Coimbatore, India, December 2009.

[17] C. Gu and Z. Wu, *Safety Monitoring of Dams and Dam Foundations-Theories Methods and Their Application*, Hohai University Press, Nanjing, China, 2006.

[18] M. Firl and K.-U. Bletzinger, "Shape optimization of thin walled structures governed by geometrically nonlinear mechanics," *Computer Methods Applied Mechanics and Engineering*, vol. 237–240, pp. 107–117, 2012.

[19] J. Fish and T. Belytschko, *A First Course in Finite Elements*, John Wiley & Sons, New York, NY, USA, 2007.

[20] O. Zienkiewicz and R. Taylor, *The Finite Element Method*, Mcgraw-Hill, London, UK, 1977.

[21] X.-S. Yang and S. Deb, "Engineering optimisation by Cuckoo search," *International Journal of Mathematical Modelling and Numerical Optimisation*, vol. 1, no. 4, pp. 330–343, 2010.

[22] R. N. Mantegna, "Fast, accurate algorithm for numerical simulation of Lévy stable stochastic processes," *Physical Review E: Statistical, Nonlinear, and Soft Matter Physics*, vol. 49, no. 5, pp. 4677–4683, 1994.

[23] E. Valian, S. Tavakoli, S. Mohanna, and A. Haghi, "Improved cuckoo search for reliability optimization problems," *Computers & Industrial Engineering*, vol. 64, no. 1, pp. 459–468, 2013.

[24] J. Kennedy and R. Eberhart, "Particle swarm optimization," in *Proceedings of the International Conference on Neural Networks (ICNN '95)*, pp. 1942–1948, IEEE, 1995.

[25] Y. Shi and R. Eberhart, "Parameter selection in particle swarm optimization," in *Proceedings of the International Conference on Evolutionary Programming*, pp. 591–600, Springer, Berlin, Heidelberg, 1998.

[26] J. Jiang, M. Tian, X. Wang, X. Long, and J. Li, "Adaptive particle swarm optimization via disturbing acceleration coefficients," *Journal of Xidian University*, vol. 39, no. 4, pp. 74–80, 2012.